

This document contains the draft version of the following paper:

R. Sinha, S.K. Gupta, C.J. Paredis, P.K. Khosla. Extracting articulation models from CAD models of parts with curved surfaces. *ASME Journal of Mechanical Design*, 124(1):106-114, 2002.

Readers are encouraged to get the official version from the journal's web site or by contacting Dr. S.K. Gupta (skgupta@umd.edu).

Extracting Articulation Models from CAD Models of Parts with Curved Surfaces

Rajarishi Sinha^{*}, *Student Member, ASME*
Institute for Complex Engineered Systems
Carnegie Mellon University
Pittsburgh, PA 15213
Email: rsinha@cs.cmu.edu
Tel.: 412-268-5214
Fax: 412-268-5229

Satyandra K. Gupta, *Member, ASME*
Department of Mechanical Engineering and
Institute for Systems Research
University of Maryland
College Park, MD 20742
Email: skgupta@eng.umd.edu

Christiaan J.J. Paredis, *Member, ASME*
Institute for Complex Engineered Systems and
Department of Electrical and Computer Engineering
Carnegie Mellon University
Pittsburgh, PA 15213
Email: cjp@cs.cmu.edu

Pradeep K. Khosla, *Member, ASME*
Department of Electrical and Computer Engineering and
Institute for Complex Engineered Systems
Carnegie Mellon University
Pittsburgh, PA 15213
Email: pkk@cs.cmu.edu

^{*} Corresponding author

Abstract

In an assembly, degrees of freedom are realized by creating mating features that permit relative motion between parts. In complex assemblies, interactions between individual degrees of freedom may result in a behavior different from the intended behavior. In addition, current methods perform assembly reasoning by approximating curved surfaces as piecewise linear surfaces. Therefore, it is important to be able to reason about assemblies using exact representations of curved surfaces; verify global motion behavior of parts in the assembly; and create motion simulations of the assembly by examination of the geometry and material properties. In this paper, we present a linear algebraic constraint method to automatically construct the space of allowed instantaneous motions of an assembly from the geometry of its constituent parts. Our work builds on previous work on linear contact mechanics and curved surface contact mechanics. We enumerate the conditions under which general curved surfaces can be represented using a finite number of constraints that are linear in the instantaneous velocities. We compose such constraints to build a space of allowed instantaneous velocities for the assembly. The space is then described as a set-theoretic sum of contact-preserving and contact-breaking subspaces. Analysis of each subspace provides feedback to the designer, which we demonstrate through the use of an example assembly – a 4-part mechanism. Finally, the results of the analysis of a 4-bar linkage are compared to those from mechanism theory.

1 Introduction and Motivation

In current design practice, when a device that contains parts with curved surfaces is considered, reasoning about its behavior is usually done by analytical methods that are difficult to implement [1, 2], or by approximating all the curves as piecewise planar surfaces [3]. The approximation is usually based on past experience or on heuristics. However, such approximations may invalidate the analysis by unintentionally constraining the degrees of freedom in the device. These erroneous results propagate throughout the design process, influencing the decisions of part and assembly designers, device analysts, process engineers, and operators.

Another consideration is the reuse of the derived device models. Even in a collaborative setting, when a part or assembly from a previous design project is reused, sometimes all that is known *a priori* is the geometry of the part or assembly. Only the CAD model of the part or assembly persists across designs. Behavioral models of the part or assembly are not reused. In addition, feature-based design of complex devices requires verification of the fact that actual kinematic behavior matches the required behavior. If component models that capture the geometry as well as the physical behavior of the device can be created, it should be possible to construct system-level simulation models merely by configuring the component models [4].

The above discussion indicates a need for three capabilities that will support all aspects of the design process - creation of the ability to exactly reason with a broad class of curved surfaces; the ability to obtain kinematic models from assembly geometry; and the ability to encapsulate kinematic behavior models and CAD models in the representation of a part or an assembly. Our research supports the first two aspects, and we are currently working on a framework that supports modular simulation-based design [4].

Frameworks for the detection and representation of articulation behavior in assemblies can be restrictive. In order to generate assembly or disassembly plans for such assemblies, the designer needs to take articulation information into consideration. However, current methods of representing articulation are restricted to systems that require complete specification by the user [5] or are based on feature recognition [6]. The former are open to incorrect input by the user resulting in illegal articulation behavior. The latter do not account for incomplete geometry and incidental contacts.

Other methods exist to obtain articulation models by reasoning on the geometric representation of the artifact. Techniques have been developed to predict the instantaneous degrees of freedom from the CAD models of parts with only polygonal planar faces [3, 7]. However, when the curved parts that exist in most engineering devices are approximated as piecewise planar parts, erroneous results are possible.

In this research, we present a methodology that generalizes our earlier work on contact surfaces [8]. Previously, the instantaneous degrees of freedom at each joint were based on surface mating constraints that were in turn obtained from analyzing body to body contacts. We imposed non-penetration constraints along the boundary of each contact surface in the form of algebraic inequalities. One can show that a finite number of non-penetration conditions are representative of the entire surface in contact. Using linear programming methods, we computed instantaneous velocities and accelerations for each pair of bodies. In this article, we obtain a set of properties that must be satisfied by a general contact surface in order to preserve the linearity of the model. We describe a method by which the space of allowable motions in the assembly can be described concisely. We then describe a heuristic that can find feasible joints from the space of allowable motions.

Such a methodology can provide useful feedback to the designer. He or she can determine which components are free to move in the assembly. The procedure can be completely automated, so that there are no errors induced by user interaction. This eliminates the possibility of input errors. In addition, since the method is algebraic and uses linear programming, it is relatively fast and is valid for all possible surface contacts, unlike rule-based systems that operate on a feature level. This method will also account for contact surfaces with incomplete geometry (such as portions of planes, cylinders, or spheres).

Our method is subject to the following restrictions. The CAD models used in the analysis are assumed to model surface contacts at joints. The joint contacts induce the instantaneous degrees of freedom. Since the algorithms detect the instantaneous degrees of freedom, they are applicable for a single configuration of a mechanism, and cannot be used to predict all possible configurations of the mechanism.

2 Review of Previous Work

2.1 Early Work on Contact Mechanics

Previous work on planar contact mechanics and screw theory prepared the foundation for this work. Ohwovoriole and Roth [9] showed that unidirectional constraints can be modeled as screws. Hirai and Asada [7] described the allowable motions of a part using polyhedral convex cones to represent the space of movement. Mattikalli and Khosla [10] described a method to obtain degrees of

freedom from component mating constraints, wherein they use a unit sphere to represent the space of all available degrees of freedom.

Some issues have not yet been addressed satisfactorily in these frameworks. Current shortcomings in articulation research include:

1. Only bodies described (or approximated) by planar surfaces are considered.
2. Current techniques are local; global interaction (propagation of constraints beyond the point where they are induced) is not satisfactory.
3. Current simulation techniques do not detect incorrect/incomplete inputs; there is no verification for correctness of the articulation representation and for the compound effect of geometric interactions and physics-based interactions.

2.2 Contact Mechanics for Planar Contacts

A part in an assembly is in physical contact with one or more other parts. The nature of these contacts can provide useful information about the types of the degrees of freedom at these contact points. Some of these contacts induce surface mating constraints, leading to the formation of a joint. Other contacts are *incidental*, in that they may bound the values of the degrees of freedom of the joint [6, 11]. Reasoning about these constraints provides the designer with valuable insight into the instantaneous degrees of freedom of the assembly.

Other researchers [3, 10] have worked with polygonal bodies and polygonal surfaces of contact. They approximate curved planar boundaries using straight lines, and use linear programming techniques to solve the contact problem.

When a pair of parts are in contact with each other, it implies that there is no inter-penetration between the parts at the contact surfaces. Penetration of one part into the other requires that the relative velocity at all the points of contact between a parts This *non-penetration condition* at a point can be written as [3]:

$$(\vec{v} + \vec{\omega} \times \vec{r}) \cdot \vec{n} \geq 0 \quad (1)$$

where \vec{v} is the relative translational velocity between two parts, $\vec{\omega}$ is the relative angular velocity between two parts, \vec{r} is the position of the point and \vec{n} is the normal at a point of contact on the surface of contact. This equation is linear in \vec{v} and $\vec{\omega}$. We define the *generalized velocity vector* as $[\vec{v} \ \vec{\omega}]$.

In Figure 1, we show the operation of the non-penetration condition at a point of contact between two planar surfaces 1 and 2, that are part of body 1 and body 2, respectively. Point P_1 is on surface 1, and is in contact with point P_2 on surface 2. \vec{n} is the surface normal at P_1 , \vec{v} and $\vec{\omega}$ are the relative translational and rotational velocities of the body pair. \vec{r} is the position vector of the contact point P_1 (or P_2).

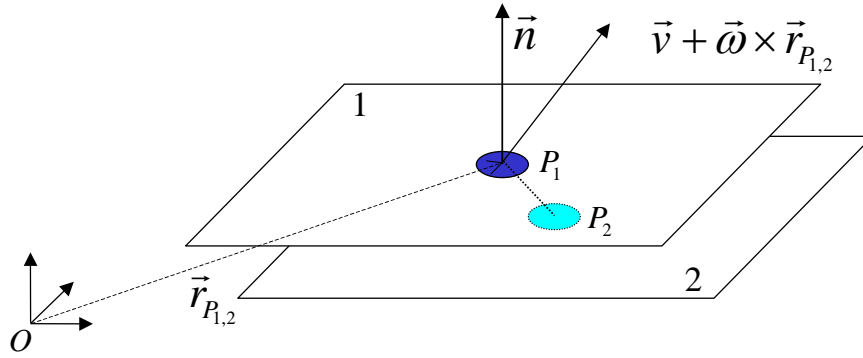


Figure 1. Non-penetration condition at a point. Planes 1 and 2 are coplanar but are shown as separated for clarity.

Figure 2 shows the non-penetration condition along a line segment from P_1 to Q_1 . For non-penetration at every point on this line segment, it is sufficient that Equation (1) be satisfied at P_1 and Q_1 .

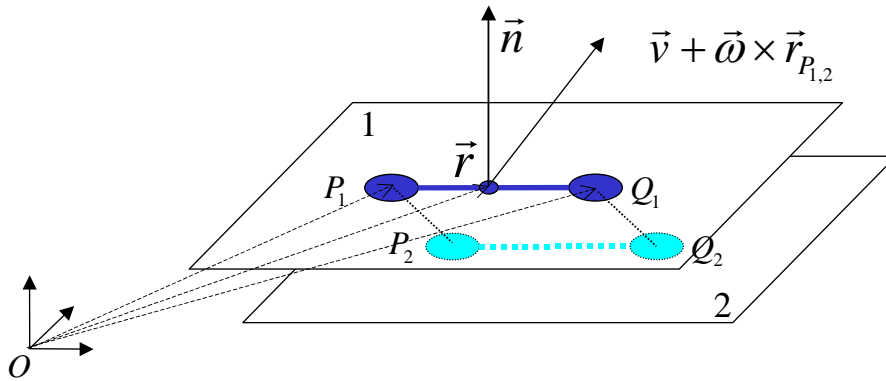


Figure 2. Non-penetration condition along a line. \vec{r} is the position vector of an arbitrary point along the contact line between P_1 and Q_1 . Planes 1 and 2 are coplanar but are shown as separated for clarity.

To prevent the penetration of one part into the other, Equation (1) must be satisfied at every point on the surface of contact and on the boundary of the surface of contact. Such a method of expressing planar contact between two bodies has been used before. For example, Mattikalli et al. [3] use non-penetration conditions to determine the impending motion direction of polyhedral rigid bodies in contact.

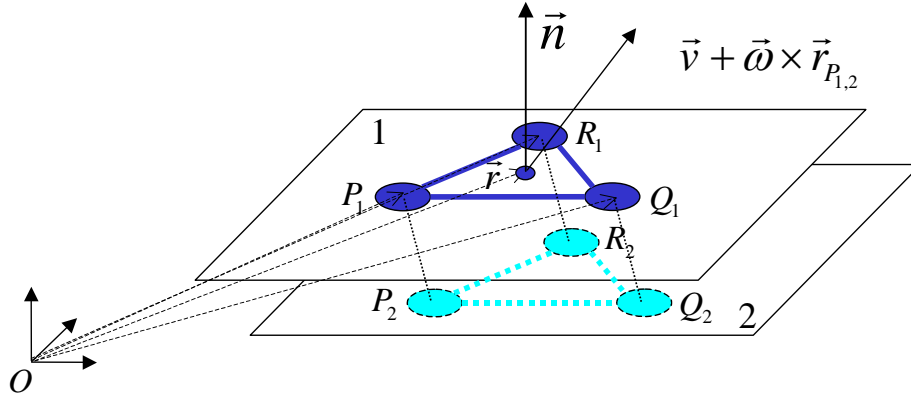


Figure 3. Non-penetration condition in a polygonal surface. \vec{r} is the position vector of an arbitrary point within the polygon bounded by P_1 , Q_1 and R_1 . Planes 1 and 2 are coplanar but are shown as separated for clarity.

We define a *primitive contact patch* to be a contact surface that is part of a single type of surface. A *compound contact patch* is an aggregation of two or more primitive patches. A closed planar patch is bounded by a finite set of curves; these curves may be straight line segments (Figure 3) or curved line segments. Any point in the interior of the patch can be expressed as a linear combination of points at the vertices of the boundary of the convex hull of the patch. Therefore, the non-penetration condition at any point in the interior can be expressed as a linear combination of the non-penetration conditions at the vertex points. As long as the convex hull has a finite number of vertices, there will be a finite number of non-penetration conditions, all of which are linear in \vec{v} and $\vec{\omega}$.

When extending to curved surface contacts, it is desirable to preserve the linearity of the formulation for reasons of computational efficiency; linearity allows for easier search and boundary enumeration.

2.3 Extending Contact Mechanics to Curved Surfaces

In a previous paper [8], we extended the results obtained for planar surface contacts by showing that similar results can also be obtained for spherical and cylindrical surfaces defined by edges that are great arcs (for spherical surfaces) or straight lines and circular arcs (for cylindrical surfaces).

Spherical surfaces in contact always result in unconstrained rotations, because they share a common center. As before, the non-penetration conditions must be written at the vertices of the convex hull for the given spherical contact surface. However, since the cost of computing the convex hull is high, we chose to generate the non-penetration condition at the vertices of the spherical patch. This will not influence the final result.

For cylindrical surfaces, non-penetration at every point in a contact patch with boundary segments that are exclusively straight line (constant- z) and circular (constant- θ) segments can be represented entirely by non-penetration at the vertices of these segments.

3 Generalized Contact Mechanics

In the previous section, we indicated that the linear properties of planar contact mechanics models can be preserved when curved surface contacts are modeled. This is possible if the contact surface boundary can be described by a finite number of segments such that satisfying the non-penetration condition the end points of the segments is necessary and sufficient to satisfy the condition at any point on the curved surface. This section defines and proves the necessary conditions.

The nature of the physical contact between a pair of parts in an assembly provides useful information about the types of the degrees of freedom. Some of these contacts induce surface mating constraints, leading to the formation of a joint. Other contacts are *incidental*, in that they bound the values of the degrees of freedom of the joint. A contact implies that non-penetration between the parts at every point on the contact surface. Non-penetration conditions can be written as inequalities that are linear in the instantaneous velocity, which when taken together, describe a linear subspace.

The following Proposition will be used to establish a theoretical basis for the linear treatment of curved surfaces in assembly modeling.

Proposition 1. *Given:*

1. *A continuous curve $C(\lambda) : \lambda \in [0,1] \rightarrow \mathfrak{R}^3$.*
2. *$C(0) = P_1$ and $C(1) = P_2$; $P_1, P_2 \in \mathfrak{R}^3$*
3. *C lies on a parametrizable, differentiable contact surface S formed between two bodies A and B .*

Then non-penetration (by Equation (1)) at P_1 and P_2 implies non-penetration at any point on C , if and only if:

1. *C is a circular arc, possibly with infinite radius (limiting case of a straight line)*
2. *The unit normal to C at any point along C is equal to the unit normal to S at that point.*

Proof. We prove Proposition 1 by showing that given Equation (1) written at P_1 and P_2 , Equation (1) holds along a set of points between P_1 and P_2 .

Equation (1) written at P_1 is:

$$(\vec{v} + \vec{\omega} \times \vec{r}_1) \bullet \vec{n}_1 \geq 0 \quad (2)$$

and at P_2 is:

$$(\vec{v} + \vec{\omega} \times \vec{r}_2) \bullet \vec{n}_2 \geq 0 \quad (3)$$

where \vec{v} is the relative translational velocity between the bodies A and B , $\vec{\omega}$ is the relative angular velocity between the two bodies, \vec{r}_1 and \vec{r}_2 are the position vectors of P_1 and P_2 , respectively. \vec{n}_1

and \vec{n}_2 are the normals to \mathbf{S} at P_1 and P_2 respectively. Forming a linear combination of Equation (2) and Equation (3), we get:

$$\lambda(\vec{v} + \vec{\omega} \times \vec{r}_1) \cdot \vec{n}_1 + (1 - \lambda)(\vec{v} + \vec{\omega} \times \vec{r}_2) \cdot \vec{n}_2 \geq 0 \text{ with } \lambda \in [0,1] \quad (4)$$

Rearranging terms in Equation (4), we get:

$$(\lambda\vec{n}_1 + (1 - \lambda)\vec{n}_2) \cdot \vec{v} + \lambda\vec{n}_1 \cdot \vec{\omega} \times \vec{r}_1 + (1 - \lambda)\vec{n}_2 \cdot \vec{\omega} \times \vec{r}_2 \geq 0 \quad (5)$$

For Equation (5) to be true and of the form of Equation (1), the following would have to be true $\forall \vec{v}, \vec{\omega}$:

$$\vec{n} = \lambda\vec{n}_1 + (1 - \lambda)\vec{n}_2 \quad (6)$$

and

$$\lambda\vec{n}_1 \cdot \vec{\omega} \times \vec{r}_1 + (1 - \lambda)\vec{n}_2 \cdot \vec{\omega} \times \vec{r}_2 = \vec{n} \cdot \vec{\omega} \times \vec{r} \quad (7)$$

Equation (6) is an expression which indicates that \vec{n} only spans the normals from \vec{n}_1 to \vec{n}_2 . By substituting Equation (6) in Equation (7) and using the vector identity $\vec{A} \cdot \vec{B} \times \vec{C} = \vec{B} \cdot \vec{C} \times \vec{A}$ to rearrange terms, we get:

$$\vec{\omega} \cdot (\vec{r}_1 \times \lambda\vec{n}_1 + \vec{r}_2 \times (1 - \lambda)\vec{n}_2) = \vec{\omega} \cdot \{ \vec{r} \times (\lambda\vec{n}_1 + (1 - \lambda)\vec{n}_2) \} \quad (8)$$

Equation (8) is true if $\vec{\omega} = \vec{0}$ (the trivial case for no rotational motion). For Equation (8) to be also true for $\vec{\omega} \neq \vec{0}$, it is sufficient to show that:

$$\lambda\vec{n}_1 \times \vec{r}_1 + (1 - \lambda)\vec{n}_2 \times \vec{r}_2 = \{ \lambda\vec{n}_1 + (1 - \lambda)\vec{n}_2 \} \times \vec{r} \quad (9)$$

Equation (9) is an expression for the generatrix or *trace* [12] \vec{r} of \mathbf{C} that generates a locus of points where Equation (1) is satisfied, given that it is satisfied at P_1 and P_2 . Taking the dot product of Equation (9) with \vec{n}_1 and \vec{n}_2 and rearranging terms, we get:

$$\begin{aligned} \{ \vec{r} - \vec{r}_1 \} \cdot (\vec{n}_1 \times \vec{n}_2) &= 0 \\ \{ \vec{r} - \vec{r}_2 \} \cdot (\vec{n}_1 \times \vec{n}_2) &= 0 \end{aligned} \quad (10)$$

Thus, for non-planar contacts, \vec{r} lies in the plane containing both P_1 and P_2 and normal to the vector $\vec{n}_1 \times \vec{n}_2$. For planar contacts (the trivial case), $\vec{n}_1 = \vec{n}_2 = \vec{n}$ and Equation (5) reduces to:

$$(\vec{v} + \vec{\omega} \times (\lambda\vec{r}_1 + (1 - \lambda)\vec{r}_2)) \cdot \vec{n} \geq 0 \quad (11)$$

Which is of the same form as Equation (1). Properties 1 and 2 are then satisfied, and *Proposition 1* is proved.

For the nontrivial case, assuming that $\vec{n}_1 \times \vec{n}_2$ is a non-zero vector, we can then parameterize \vec{r} as (see Figure 4):

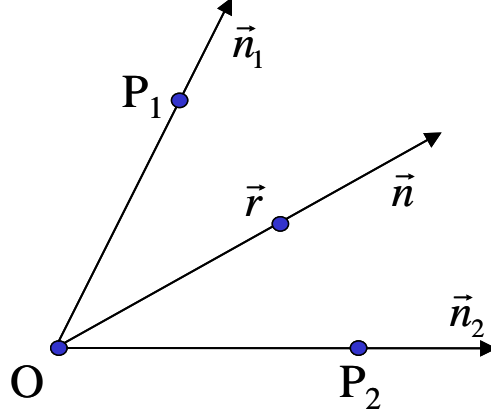


Figure 4. Plane containing \vec{r} also contains the normal vectors to \vec{r} .

$$\vec{r} = \vec{o} + \alpha \frac{\vec{n}}{\|\vec{n}\|} \text{ and } \vec{n} = \beta \vec{n}_1 + (1 - \beta) \vec{n}_2 \quad (12)$$

Where \vec{o} is an arbitrary origin. Using Equation (12) to substitute for \vec{r} , \vec{r}_1 and \vec{r}_2 in Equation (9) and expanding, we get:

$$\alpha \frac{\vec{n}_1 \times \vec{n}_2}{\|\vec{n}\|} [\lambda - \beta] = \vec{0} \quad (13)$$

From Equation (13), it follows that since $\vec{n}_1 \times \vec{n}_2$ cannot be zero (as per our assumption), λ is equal to β . In all of the subsequent analysis, we will use β , with the understanding that the parameterizations by λ and β are equivalent.

The curve described in Equation (12) must lie on the specified surface \mathbf{S} . This is equivalent to saying that the tangent vector to the curve at every point on the curve must be perpendicular to the normal to the surface and the normal vector to the curve must be parallel to the normal vector to the surface. We enforce this by the following constraint on \mathbf{C} :

$$\frac{d\vec{r}}{ds} \bullet \vec{n}(s) = 0 \quad (14)$$

where s is the arc length, and $\vec{n}(s)$ is the normal vector field. Substituting from Equation (12):

$$\frac{d\vec{r}}{ds} = \frac{d\alpha}{ds} \left(\frac{\vec{n}}{\|\vec{n}\|} \right) + \alpha \left(\frac{\|\vec{n}\| \frac{d\vec{n}}{d\beta} - \vec{n} \frac{1}{\|\vec{n}\|} \left(\vec{n} \bullet \frac{d\vec{n}}{d\beta} \right)}{\|\vec{n}\|^2} \right) \frac{d\beta}{ds} \quad (15)$$

or, upon simplification and substitution of Equation (15) in Equation (14):

$$\frac{d\vec{r}}{ds} \bullet \vec{n}(s) = \frac{d\alpha}{ds} \|\vec{n}\| = 0 \quad (16)$$

which implies that:

$$\alpha(s) = \text{constant} \quad (17)$$

With Equation (17), Equation (12) reduces to that of a circular arc in the plane. The unit normal vector to any point on this arc is equal to the unit normal vector to the surface \mathbf{S} at that point. This established properties 1 and 2, and proves *Proposition 1*.

To prove the converse, i.e. given a circular arc lying on the surface \mathbf{S} with the unit normal vector field to the arc equal to the unit normal vector field of the surface, we write Equations (2) and (3) for a circular arc. Thus Equation (2) becomes:

$$(\vec{v} + \vec{\omega} \times (\vec{o} + R\vec{n}_1)) \bullet \vec{n}_1 \geq 0 \quad (18)$$

and Equation (3) becomes:

$$(\vec{v} + \vec{\omega} \times (\vec{o} + R\vec{n}_2)) \bullet \vec{n}_2 \geq 0 \quad (19)$$

where R is the radius of the circular arc. Expanding Equations (18) and (19) and forming a linear combination:

$$(\vec{v} + \vec{\omega} \times \vec{o}) \bullet (\lambda\vec{n}_1 + (1-\lambda)\vec{n}_2) \geq 0 \quad (20)$$

which is of the same form as Equation (1). Therefore, non-penetration at the points P_1 and P_2 implies non-penetration all along \mathbf{C} . Note that this is similar to the proof of non-penetration along a circular arc on a right circular cylinder, presented in Sinha et al. [8]. This completes the proof of *Proposition 1*.

Lemma 1.1. *The curve \mathbf{C} exists on surface \mathbf{S} when:*

1. $(\vec{r}_1 - \vec{r}_2) \bullet (\vec{n}_1 \times \vec{n}_2) = 0$
2. *The intersection of \mathbf{S} with the above plane is a circular arc.*

Proof. The above two conditions follow from *Proposition 1*. Curve \mathbf{C} lies in a plane containing the points P_1 and P_2 , as defined in Equation (10). \mathbf{C} is also a circular arc on \mathbf{S} , as shown in Equation (17).

Corollary 1.1. *The straight line $l(\lambda) : \lambda \in [0,1] \rightarrow \lambda\vec{r}_1 + (1-\lambda)\vec{r}_2$ on a plane surface \mathbf{S} satisfies *Proposition 1*.*

Corollary 1.2. *The great arc on a spherical surface \mathbf{S} subtending an angle less than π satisfies *Proposition 1*.*

Corollary 1.3. *The straight vertical line parallel to the axis and the circular arc subtending an angle less than π on a right circular cylindrical surface \mathcal{S} satisfies Proposition 1.*

Proof. Corollaries 1.1 through 1.3 are discussed and proved individually in Sinha et al. [8]. Here, we show that they emerge as special cases of *Proposition 1*. As per the Proposition, the only possible segment on a planar surface (Corollary 1.1), with \vec{n}_1 equal to \vec{n}_2 , is the circular arc with infinite radius, i.e. the straight line joining the points P_1 and P_2 . The great arc on a spherical surface also satisfies *Proposition 1*. The possible segments on a right circular cylindrical surface are the vertical straight line and the circular arc. The subtended angle is required to be less than π to prevent \vec{n}_1 being parallel to \vec{n}_2 .

Corollary 1.4. *The straight vertical line starting at the apex of a right conical surface \mathcal{S} satisfies Proposition 1.*

Proof. Upon examination of a right circular conical surface, we see the straight line (or meridian lines) of the cone has its unit normal vector equal to the unit normal vector of the surface of the cone. Therefore, *Proposition 1* is satisfied. Note that circular arcs can be present on the cone, but do not satisfy *Proposition 1* because the unit normals along the arc do not point in the same direction as the normal vectors of the cone.

4 Articulation in Assemblies

This section describes how the space of allowed motion is computed from the non-penetration conditions, and how the model of the space can be queried to provide designer feedback. When an unconstrained degree of freedom exists, the space of allowed instantaneous motion generated from the non-penetration conditions will be non-empty. The space can be analyzed to provide feedback to the designer.

4.1 Solving the Set of Non-Penetration Conditions for Instantaneous Articulation

Each primitive patch induces a non-penetration condition at each of its (finite) vertices. Since penetration must not occur at any point at any time, the inequalities for all the non-penetration conditions for the all the patches of a pair of bodies considered simultaneously form the linear program:

$$\vec{n}_i \bullet (\vec{v} + \vec{\omega} \times \vec{r}_i) \geq 0 \quad i = 1 \dots \text{Total number of vertices in all patches} \quad (21)$$

where \vec{v} and $\vec{\omega}$ are the relative velocities between the two parts, \vec{n}_i is the normal at each vertex and \vec{r}_i is the position of each vertex.

Since at any time, *all* the non-penetration conditions for all the parts must be satisfied, it is possible to solve all the inequalities for all the vertices of all the parts in the same linear program. This will result in a solution that is globally valid. Using a single linear program, it is possible to obtain all the instantaneous degrees of freedom for the assembly. If we write the non-penetration condition for a patch concisely as:

$$\mathbf{J}_{patch} \begin{bmatrix} \vec{v}_A - \vec{v}_B \\ \vec{\omega}_A - \vec{\omega}_B \end{bmatrix} \geq \vec{0} \quad (22)$$

where \mathbf{J}_{patch} is the non-penetration inequality coefficient matrix for that particular patch. Then the non-penetration conditions for all the patches in a body-body contact pair formed between bodies A and B can be written as:

$$\mathbf{J}_{AB} \begin{bmatrix} \vec{v}_A - \vec{v}_B \\ \vec{\omega}_A - \vec{\omega}_B \end{bmatrix} = \begin{bmatrix} \mathbf{J}_{patch_1} \\ \mathbf{J}_{patch_2} \\ \vdots \\ \mathbf{J}_{patch_p} \end{bmatrix} \begin{bmatrix} \vec{v}_A - \vec{v}_B \\ \vec{\omega}_A - \vec{\omega}_B \end{bmatrix} \geq \vec{0} \quad (23)$$

where p is the number of patches in which this body-body pair participates. Writing Equation (23) for all the body-body contact pairs in an assembly, we get:

$$\mathbf{J}_{assembly} \begin{bmatrix} \vec{v}_A \\ \vec{\omega}_A \\ \vec{v}_B \\ \vec{\omega}_B \\ \vdots \end{bmatrix} = \begin{bmatrix} \mathbf{J}_{AB} & -\mathbf{J}_{AB} & \mathbf{0} & \cdots & \mathbf{0} \\ \mathbf{0} & \mathbf{J}_{BC} & -\mathbf{J}_{BC} & \cdots & \mathbf{0} \\ \vdots & \vdots & \vdots & \ddots & \vdots \end{bmatrix} \begin{bmatrix} \vec{v}_A \\ \vec{\omega}_A \\ \vec{v}_B \\ \vec{\omega}_B \\ \vdots \end{bmatrix} \geq \vec{0} \quad (24)$$

where $\mathbf{J}_{assembly}$ is a complete representation of the assembly with instantaneous articulation. Solving this global simplex provides all the translational and angular velocities for all the body-body pairs simultaneously.

The simplex is $6N-6$ -dimensional (3 variables for translational velocity and 3 variables for angular velocity for each of $N-1$ ungrounded bodies in the assembly). Since the origin is a vertex of this high-dimensional space, this structure is also called a Polyhedral Convex Cone. Such structures have been studied extensively by Goldman and Tucker [13] and others. Hirai and Asada [7] used cones to describe the possible contact-preserving and contact-breaking motions between two polyhedral bodies.

4.2 A CAD Implementation for Instantaneous Articulation

Having established a theoretical framework for treating curved surface contacts in the previous sections, we now describe the system that extracts non-penetration conditions from the CAD models of parts in an assembly. A *contact graph* structure \mathbf{G} can be used to represent the assembly (Figure 5). In the contact graph, parts are represented as nodes, and contacts between parts are represented as edges between the corresponding nodes. Edges between nodes are automatically derived by performing intersections between the corresponding parts.

$$G = \{(A, B, I) : A, B \in \text{Set of parts}; A \neq B; I = \text{Result of intersection between A and B}\} \quad (25)$$

where G is the contact graph that contains a finite number of 3-tuples. Each 3-tuple contains two parts and an intersection set.

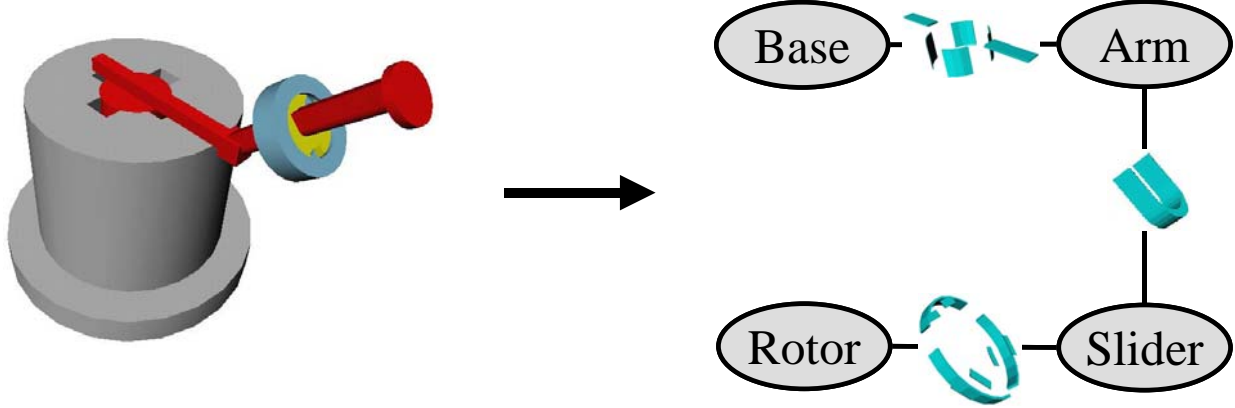


Figure 5. Contact graph for a 4-part assembly. Nodes represent the four parts. Edges represent the contacts. The contact surface that forms the intersection set is shown in each edge.

The intersection information in each edge is examined for features that could indicate the presence of surface mating constraints. Each element of I can be thought of as a *constraint patch* on the mating surface between A and B . For a particular element, all boundary segments that do not satisfy *Proposition 1* are discretized into *primitive segments* (straight lines on planes, circular arcs and straight lines on a cylinder for constant z and constant θ respectively, and great arcs on a sphere), each of which satisfy *Proposition 1*. The set I can be partitioned as:

$$I = \underbrace{S_1 \cup S_2 \cup S_3 \cup \dots \cup S_n}_{\text{finite } n} \quad (26)$$

where S_1 through S_n are a finite number of *primitive surfaces* (or patches). On each S , there exists a finite set of boundary segments Ω :

$$\Omega = \{\sigma : \sigma \in \text{Set of boundary segments of } S\} \quad (27)$$

$$\text{s.t. } \sigma \approx \hat{\sigma} = \underbrace{\alpha_1 \cup \alpha_2 \cup \dots \cup \alpha_m}_{\text{finite } m}$$

where σ is either a primitive segment, or can be approximated as $\hat{\sigma}$ which is a union of a finite number of primitive segments α . Thus, the intersection set I is composed of a finite number of primitive boundary segments.

The non-penetration condition for each end-point or vertex of each primitive boundary segment α is written as a constraint in the linear program. The linear space can now be described (or enumerated) using standard boundary enumeration techniques. Note that this technique will work only for those surfaces that satisfy *Proposition 1*. On other surfaces such as splines, non-penetration conditions would have to be written for every point on the surface.

Finding one solution to the simplex is easy; finding *all* solutions is a more difficult proposition. However, useful information can still be obtained by projecting the simplex on either the \vec{v} , or the $\vec{\omega}$ space. Such linear programming methods have previously been used by Mattikalli et al. [3] to obtain solutions to the stability problem for assemblies.

Solutions are returned in the form of allowable instantaneous translational and angular velocities. Translational velocities of zero indicate that translation is constrained for that body-body pair. Angular velocities of zero indicate that rotation is constrained for that body-body pair.

4.3 Giving Feedback to the Designer

In order to completely describe all the possible relative motions of the assembly, it is necessary to completely describe the boundary of the polyhedral convex cone in $6N-6$ -dimensional space.

Useful feedback can be provided to the designer in the form of questions such as: “What degrees of freedom exist when the rotations of a particular part are constrained?” This question can be answered by adding $\vec{\omega} = \vec{0}$ for the body in question, to the set of constraints and evaluating the linear program. Other possible “what-if” analyses include grounding a part (i.e. setting $\vec{v} = \vec{0}$ and $\vec{\omega} = \vec{0}$ for that part) and obtaining the instantaneous degrees of freedom for all the other parts.

The space of allowed motions can be represented by the set-theoretic sum of the space of motions that preserve the contact ($J_{assembly} \vec{V} = \vec{0}$), and the space of motions that break the contact ($J_{assembly} \vec{V} > \vec{0}$), where \vec{V} is the vector of generalized velocities:

$$S_{allowed} = S_{contact-preserving} + S_{contact-breaking} \quad (28)$$

$S_{contact-preserving}$ is the space of possible generalized velocity vectors that cause all contacts to be maintained, or:

$$S_{contact-preserving} = Nullspace(J_{assembly}) \quad (29)$$

The basis vectors of the nullspace completely describe the possible contact-preserving motions. A singular value decomposition of $\mathbf{J}_{assembly}$ is used to compute the nullspace.

Computing the boundary of the space of contact-breaking motions is a much harder problem. Avis [14], Avis and Fukuda [15, 16], Motzkin et al. [17], Bremner et al. [18], and Fukuda and Prodon [19] have all proposed methods to enumerate the boundary of a polyhedral convex cone. However, time requirements for these methods quickly explode when confronted with cones of increasing dimensionality. Nemhauser and Wolsey [20] show that the extreme ray membership problem for a cone is in NP. Similar conclusions are drawn by Avis [21]. For a discussion of the complexity class of enumeration problems see Fukuda [22].

Given a cone, it is possible to verify the feasibility of a given solution in polynomial time [20]. Therefore, we propose the following heuristic to construct a finite set of feasible solutions from the geometry of the assembly:

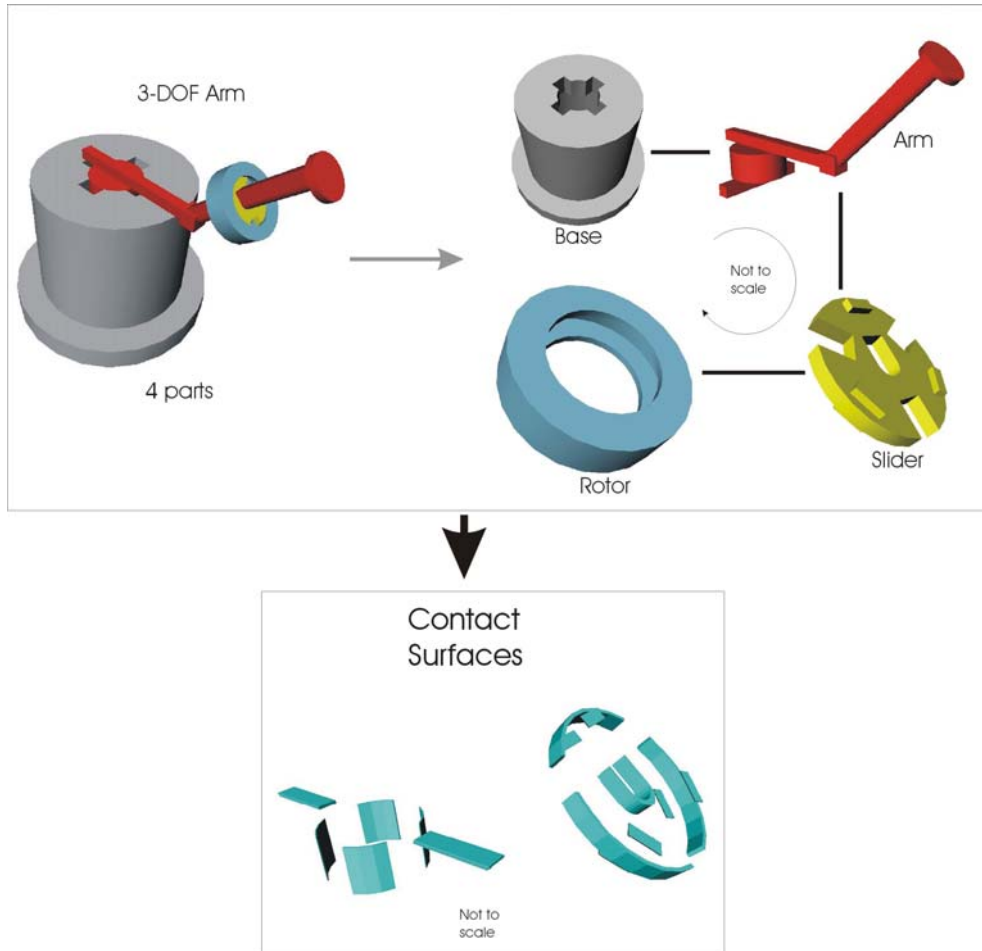


Figure 6. 4-part assembly with 3 degrees of freedom.

1. For every primitive contact patch, pick the axis and a position on the axis - for planes, the normal to the plane; for cylinders and cones, the principal axis; for spheres, any axis; in addition, pick a second axis tangent to the direction of curve parameterization - for planes, an axis lying in the plane, for cylinders and cones, the axis of the base; for spheres, any axis perpendicular to the first axis.
2. See if a translational velocity along and/or a rotational velocity about these axes are feasible solutions to the set of non-penetration conditions.
3. Since there are a finite number of patches, therefore a finite number of axes, the number of possible feasible solutions will be finite. Note that this heuristic will fail to detect degrees of freedom that are not along axes of symmetry.

Introduction of domain-specific knowledge (geometric information, in this case), enables us to draw useful inferences about the space of allowed motions. The feasible solutions that emerge from this test, along with the nullspace of the cone, form a representation of the cone. Feasible solutions for a particular pair of parts can be combined to form joints between parts.

5 Illustrative Examples

5.1 Example 1 (Arm): Demonstration of the Framework

In order to illustrate the framework defined in the previous sections, we present an example assembly. The assembly in **Error! Reference source not found.** is a 4-part assembly, with three functional degrees of freedom. We choose to render the base immobile (i.e. we *ground* it), by constraining all the six degrees of freedom.

The system is implemented in C++, using ACIS as a solid modeller, and with Open Inventor for 3-D visualization. This example problem was solved on a SUN Ultra-2 computer running Solaris 7, using 16 seconds of CPU time, from input of the CAD models to output of the joint information for the assembly.

Contact analysis indicates that this is an open-chain assembly, with 9 linear-boundary planar contacts (base-to-arm, arm-to-slider and slider-to-rotor), 1 curved-boundary planar contact (base-to-arm), 8 partial cylindrical contacts (base-to-arm, arm-to-slider and slider-to-rotor). This generates a total of 81 inequalities, linear in 18 variables forming the relative translational and rotational velocities (assuming the base is grounded).

The 81 constraints define a polyhedral convex cone in 18-dimensional space (see Figure 7). The matrix representation can be partitioned into two: the nullspace and the interior boundary enumeration representation. Singular value decomposition returns a rank of 15, indicating that there are three completely unconstrained degrees of freedom (and as a result, the nullspace is 3-dimensional). The nullspace basis $[N_1, N_2, N_3]$ is shown in Equation (30).

$$\begin{aligned} N_1 &= [0 \ 0 \ 0 \ 0 \ 0 \ 0 \ 1 \ 0 \ 1 \ 0 \ 0 \ 0 \ 1 \ 0 \ 1 \ 0 \ 0 \ 0] \\ N_2 &= [0 \ 0 \ 0 \ 0 \ 0 \ 0 \ 0 \ 0 \ 0 \ 0 \ 0 \ 0 \ 0 \ 0 \ -17 \ 0 \ 1 \ 0 \ 1] \\ N_3 &= [0 \ 0 \ 0 \ 0 \ 0 \ 1 \ 0 \ 0 \ 0 \ 0 \ 0 \ 1 \ 0 \ 0 \ 0 \ 0 \ 0 \ 1] \end{aligned} \quad (30)$$

where

$$N_i = \left[\underbrace{v_x \ v_y \ v_z \ \omega_x \ \omega_y \ \omega_z}_{Arm} \ \underbrace{v_x \ v_y \ v_z \ \omega_x \ \omega_y \ \omega_z}_{Slider} \ \underbrace{v_x \ v_y \ v_z \ \omega_x \ \omega_y \ \omega_z}_{Rotor} \right]$$

Nullspace basis vector N_1 indicates the presence of a translational degree of freedom for the slider and rotor with respect to the base. This freedom is at a 45° angle to the horizontal plane, indicated by the equal infinitesimal relative translational motions in the x and z directions. Basis vector N_2 indicates that there is a relative instantaneous rotation of the rotor with respect to the base at a 45° angle to the horizontal plane. The $[0 \ -17 \ 0]$ translational component stems from the fact that the instantaneous rotation is not about the origin, but instead about the axis $[1 \ 0 \ 1]$ through the point $[18 \ 0 \ 1]$.

For the instantaneous velocity of the body to be zero at the point $[18 \ 0 \ 1]$,

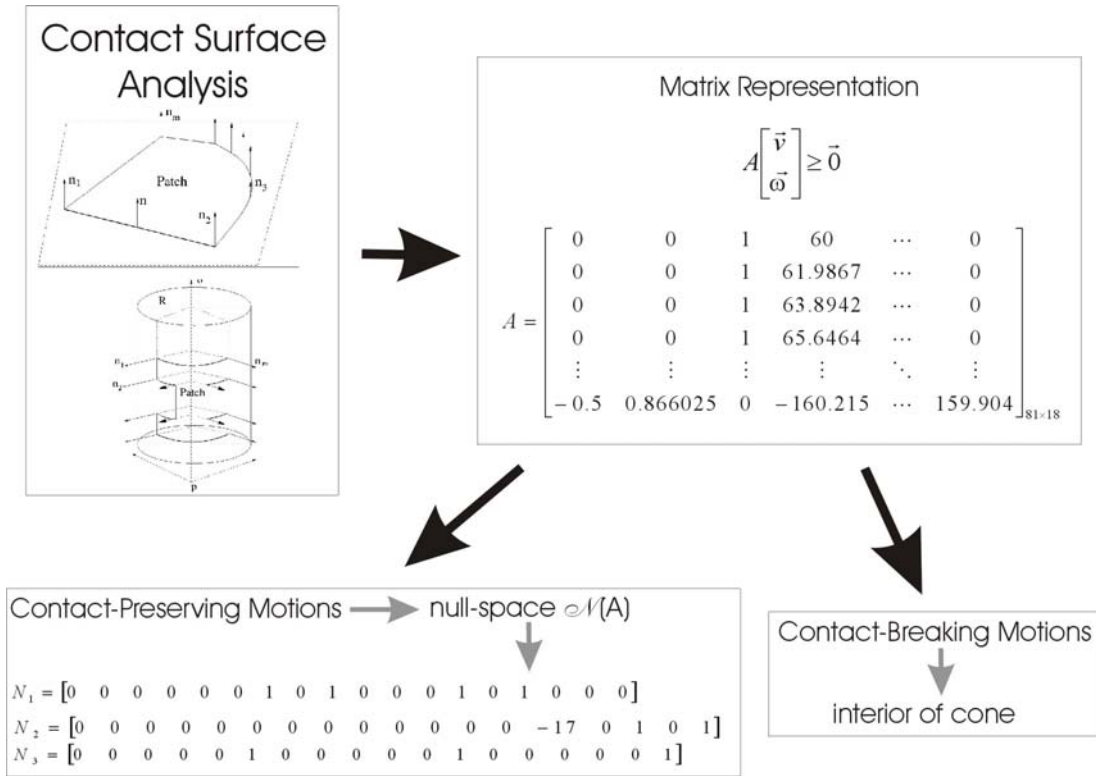


Figure 7. Formation of the Matrix Representation.

$$\vec{v}_{total} = \vec{v}' + \vec{\omega} \times \vec{p} = \vec{0} \quad (31)$$

or:

$$\vec{v}' = \vec{p} \times \vec{\omega} = [0 \quad -17 \quad 0] \quad (32)$$

where \vec{v}' is the translational component, namely $[0 \quad -17 \quad 0]$; $\vec{\omega}$ is the instantaneous angular velocity component, namely $[1 \quad 0 \quad 1]$; and \vec{p} is the locus of positions that satisfies Equation (32). Thus, we get an axis $[1 \quad 0 \quad 1]$ passing through $[18 \quad 0 \quad 1]$. Thus, nullspace analysis describes the boundary of the cone.

Feasible solutions are constructed from the contact patches. The 18 primitive patches result in 216 candidate feasible solutions. Each candidate is tested to determine if it is within the space of allowed instantaneous motion. Four candidates are found to be valid solutions. Of the four valid solutions, three are identical to the nullspace basis vectors. The fourth is $[0 \quad 0 \quad 1 \quad 0 \quad 0 \quad 0 \quad 0 \quad 1 \quad 0 \quad 0 \quad 0 \quad 0 \quad 0 \quad 1 \quad 0 \quad 0 \quad 0]$, corresponding to the contact-breaking motion (vertical translation along the z-axis) between the base and the other 3 parts.

Once valid feasible solutions are available, it is possible to group them together to define joints between parts in the assembly. One of the feasible solutions in this example results in a revolute joint being formed between the base and the arm (see Figure 8). This joint information is added to

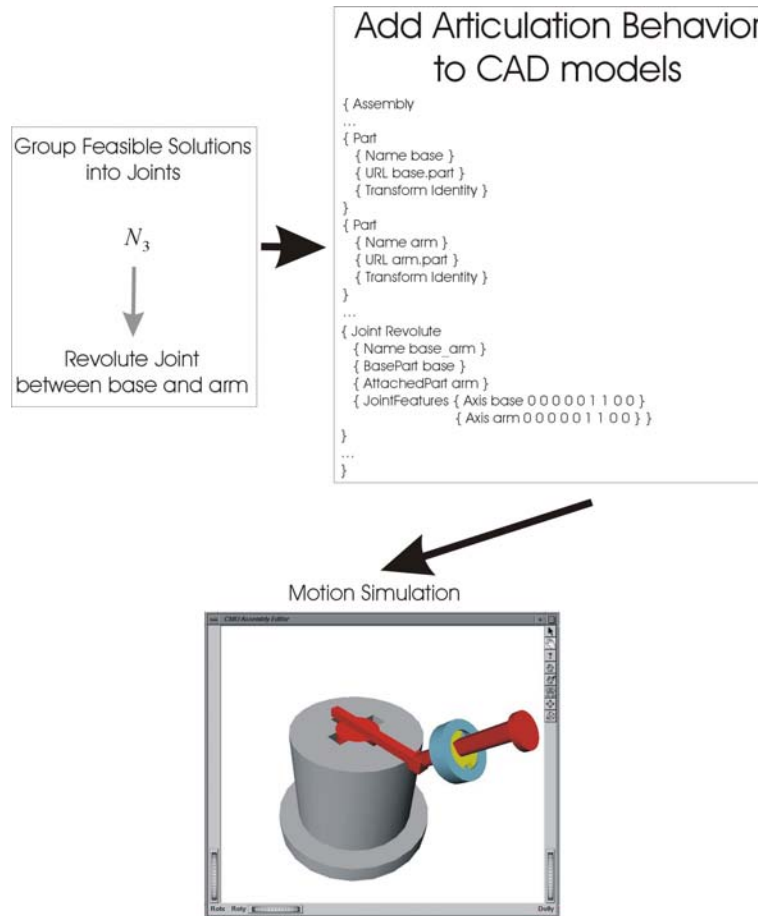


Figure 8. Mapping feasible solutions to assembly joints.

the representation of the assembly. Once joints are detected automatically, information about the material properties can be combined with kinematic information to perform motion simulations.

5.2 Example 2 (1-DOF 4-Bar Linkage): Global Constraint Resolution

To verify the correctness of our implementation, we compared the results of our system to the analytical formulation for a 4-bar linkage. The example in this subsection is a 4-bar assembly with 1 degree of freedom (see Figure 9) with each bar having a joint axis-to-joint axis distance of 39 units.

Computing the contact surfaces from the CAD model indicates that there are 4 contacts between the bars, each shaped like a “top hat”. Each top hat contact has 2 planar contact surfaces bounded by a curved boundary and 1 complete cylindrical contact surface. The two planar contact surfaces constitute the top and the rim of the hat. The cylindrical contact surface constitutes the side of the hat. The non-penetration condition is satisfied everywhere on the cylindrical contact surface if it is satisfied at 6 points at the top and bottom boundary of the surface. On the two planar contact surfaces, we select 109 points that approximate the boundaries of the surfaces, and impose the non-penetration condition at these points. This results in a total of 114 inequalities per pair of bars, for a grand total of 460 inequalities in 18 relative translational and rotational velocity variables (assuming that Bar 1 is grounded).

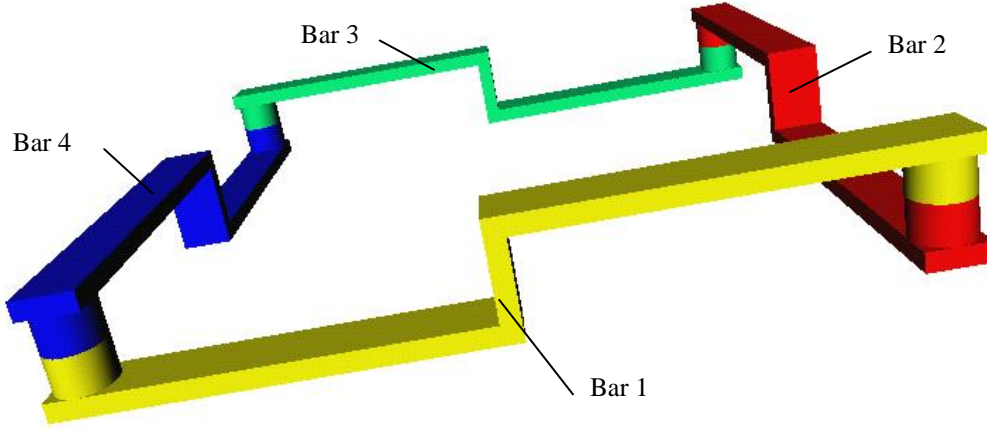


Figure 9. 4-Bar Linkage

The inequalities are used to construct the inequality coefficient matrix A (similar to the one in Figure 7). Each inequality becomes a row in the matrix, resulting in a matrix of size 460×18 . The matrix has a rank of 17. Therefore, the nullspace N is 1-dimensional, indicating the presence of 1 completely unconstrained degree of freedom. A basis vector for the nullspace of A is:

$$N_1 = [0 \quad -39 \quad 0 \quad 0 \quad 0 \quad 1 \quad -39 \quad 0 \quad 0 \quad 0 \quad 0 \quad 0 \quad 0 \quad 0 \quad 0 \quad 0 \quad 0 \quad 1] \quad (33)$$

where

$$N_1 = \left[\underbrace{v_x \quad v_y \quad v_z \quad \omega_x \quad \omega_y \quad \omega_z}_{\text{Bar 2}} \quad \underbrace{v_x \quad v_y \quad v_z \quad \omega_x \quad \omega_y \quad \omega_z}_{\text{Bar 3}} \quad \underbrace{v_x \quad v_y \quad v_z \quad \omega_x \quad \omega_y \quad \omega_z}_{\text{Bar 4}} \right]$$

Breaking one of the bar-bar contacts would have resulted in an open-chain assembly, with 3 more degrees of freedom. The closed-loop eliminates these extra degrees of freedom, and this is reflected in the 1-dimensional nullspace. Examining the nullspace, we see that for an unit instantaneous rotation of **Bar 4** with respect to **Bar 1** about the z-axis, **Bar 2** undergoes a unit instantaneous rotation about the z-axis, but at a position of $[39 \ 0 \ 0]$ (using Equation (31)). **Bar 3** undergoes an instantaneous pure translation along the x-axis of a magnitude 39 times that of the rotation.

The 4-bar linkage has been extensively studied by mechanism theorists. Its behavior is well known. From [23] (see pp. 233-234), we see that the “velocity-loop equation” written for our 4-bar linkage is:

$$\begin{aligned} L\vec{\omega}_4 - L\vec{\omega}_2 &= \vec{0} \\ L\vec{\omega}_3 &= \vec{0} \end{aligned} \quad (34)$$

where L is the length of the bar, $\vec{\omega}_2$ is the angular velocity of **Bar 2** with respect to **Bar 1**, $\vec{\omega}_3$ is the angular velocity of **Bar 3** with respect to **Bar 1**, and $\vec{\omega}_4$ is the angular velocity of **Bar 4** with respect to **Bar 1**. Thus, $\vec{\omega}_2$ is equal to $\vec{\omega}_4$ and $\vec{\omega}_3$ is zero. Since the links are rigid, for every $\delta\theta$ rotation of **Bar 2** and **Bar 4**, there must be a $L\delta\theta$ x-axis displacement of **Bar 3**. This is identical to the previous result. This validates our implementation of degree of freedom extraction.

6 Discussion

The geometry of the parts in an assembly restricts how they can be assembled, and how they move relative to one another. This in turn influences their static stability, kinematic behavior, and dynamic performance characteristics. However, models for these phenomena do not exist initially. The designer provides joint information at the conceptual design stage to meet certain functional requirements of the assembly. This information is provided either by specifying kinematic constraints between parts as annotations to the assembly CAD model, or by specifying mating conditions between specific features on the parts. It can also be derived from the CAD models of the individual parts, and from the relative positions of these parts in the final assembly. Or the information could be obtained by some combination of designer input and automatic derivation. Therefore, there can be two types of constraints between parts, namely, constraints introduced by the designer to satisfy functional requirements of the assembly, and constraints induced by the geometry of parts in the assembly. Both these types of constraints interact to produce a resultant behavior of a joint. It is important to be able to derive the joint behavior from the CAD model, as well as to verify that designer input is consistent with the CAD model.

Our method reasons on the CAD model of the assembly to obtain the instantaneous degrees of freedom. It is able to handle incomplete curved geometry, while at the same time resolving global (i.e. multi-part) constraint interactions. Linear algebra-based constraint models are derived directly from CAD models, and then converted into articulation representations suitable for assembly planning and motion simulation. A proposition and other supporting theorems enumerate the properties of the contact surfaces between the parts that must be satisfied to construct a linear algebraic constraint model.

The linear algebra-based constraint model can be used to provide designer feedback. The model describes the space of allowable instantaneous motion in the assembly. Although solving for the complete boundary of this space is thought to be in NP, whether a particular instantaneous degree of freedom is within the space can be verified in polynomial time. Therefore, our framework also supports the ability to query the model with the designer specified joint information to verify that the information is correct.

We validated our method by applying it to the 4-bar linkage, and comparing the results with those obtained from mechanism theory.

Under certain circumstances, our method breaks down: contact surfaces that are represented by polynomial or transcendental functions have to be approximated as piecewise planar, cylindrical or spherical contacts – this approximation may remove a degree of freedom. A valid candidate degree of freedom may not be detected if the freedom does not lie along an axis of symmetry. Our method is applicable only to assembly geometry that is modeled by exact CAD models without fit tolerances. The method is also only applicable to the particular mechanism configuration that is captured in the CAD model.

7 Conclusions and Future Work

This research forwards the state-of-the-art in the following ways:

Exact Treatment of Curved Geometry. Previous work on the application of linear programming techniques to the contact mechanics between two surfaces was restricted to handling planar surfaces only [3, 10]. Curved surfaces were handled by approximating them as planar facets, or by using graphical methods. This result was extended to curved surfaces whose boundaries possess certain properties. The vast majority of manufactured parts have contacts that possess such boundaries. Therefore, the work presented here allows a designer to analyze and design devices that contain parts (or components) that in turn contain a broad class of curved surfaces.

Modeling Support For Kinematics Behavior. Solving the contact conditions at the boundary will enable the designer to obtain the instantaneous degrees of freedom of the device. Using generate-and-test methods and reasoning about the geometry of the artifact will reveal the bounds on the values of the degrees of freedom. Such information, when combined with information about the mass distribution and with friction models, will allow the designer to determine the stability of the device, handle articulation during assembly planning, during synthesis of part geometry, as well as during the operation of the device.

Accurate and Automatic Simulation Synthesis. Simulation of the operation of the electromechanical device requires kinematic and dynamic information. Since the CAD model of each component incorporates such information, high-fidelity simulation can be created and executed with minimal user interaction.

Interesting research issues remain with regard to the handling of model uncertainty and in the quantification of the effect of model approximations, such as the discretization of curved planar contact boundaries, on the final result of the articulation analysis.

Acknowledgements

This research was funded in part by DARPA under contract ONR #N00014-96-1-0854, by the Raytheon Company, the National Institute of Standards and Technology, the Robotics Institute, and the Institute for Complex Engineered Systems at Carnegie Mellon University. In addition to the reviewers, we would like to thank Dr. Raju Mattikalli and Prof. Benoit Morel for their insightful feedback.

References

- [1] Ge, Q. and McCarthy, J. M., "Functional Constraints as Algebraic Manifolds in a Clifford Algebra," *IEEE Journal Robotics and Automation*, vol. 7, pp. 670-677, 1991.
- [2] Liu, Y. and Popplestone, R., "A Group Theoretic Formalization of Surface Contact," *International Journal of Robotics Research*, vol. 13, pp. 148-161, 1994.
- [3] Mattikalli, R., Baraff, D., Khosla, P., and Repetto, B., "Gravitational Stability of Frictionless Assemblies," *IEEE Transactions on Robotics and Automation*, vol. 11, pp. 374-388, 1995.
- [4] Paredis, C. J. J., Diaz-Calderon, A., Sinha, R., and Khosla, P. K., "Composable Models for Simulation-Based Design," *Engineering with Computers*, vol. in press, 2001.
- [5] ADAMS, "Http://Www.Adams.Com,"., 2000.

- [6] Rajan, V., Lyons, K., and Sreerangam, R., "Generation of Component Degrees of Freedom from Assembly Surface Mating Constraints," *1997 ASME Design Engineering Technical Conference*, Sacramento, CA, pp. 1-12, 1997.
- [7] Hirai, S. and Asada, H., "Kinematics and Statics of Manipulation Using the Theory of Polyhedral Convex Cones," *International Journal of Robotics Research*, vol. 12, pp. 434-447, 1993.
- [8] Sinha, R., Paredis, C. J. J., Gupta, S. K., and Khosla, P. K., "Capturing Articulation in Assemblies from Component Geometry," *ASME Design Engineering Technical Conference*, Atlanta, GA, 1998.
- [9] Ohwovoriole, M. S. and Roth, B., "An Extension of Screw Theory," *ASME Journal of Mechanical Design*, vol. 103, pp. 725-735, 1981.
- [10] Mattikalli, R. and Khosla, P. K., "Analysis of Restraints to Translational and Rotational Motion from the Geometry of Contact," *ASME Winter Annual Meeting*, Atlanta, pp. 65-71, 1991.
- [11] Rajan, V. N. and Noy, S. Y., "Minimal Precedence Constraints for Integrated Assembly and Execution Planning," *IEEE Trans. Robotics and Automation*, vol. 12, pp. 175-186, 1996.
- [12] Gray, A., *Modern Differential Geometry of Curves and Surfaces with Mathematica*. New York, NY: CRC Press, 1998.
- [13] Goldman, A. J. and Tucker, A. W., "Polyhedral Convex Cones," in *Linear Inequalities and Related Systems*, vol. 39, *Annals of Math Studies*, H. W. Kuhn and A. W. Tucker, Eds. Princeton, NJ: Princeton University Press, pp. 19-39, 1956.
- [14] Avis, D., "A C Implementation of the Reverse Search Vertex Enumeration Algorithm," in *Rims Kokyuroku 872*, H. Imai, Ed. Kyoto: Kyoto University, 1994.
- [15] Avis, D. and Fukuda, K., "A Pivoting Algorithm for Convex Hulls and Vertex Enumeration of Arrangements and Polyhedra," *Discrete and Computational Geometry*, vol. 8, pp. 295-313, 1992.
- [16] Avis, D. and Fukuda, K., "Reverse Search for Enumeration," *Discrete Applied Mathematics*, vol. 6, pp. 21-46, 1996.
- [17] Motzkin, T. S., Raiffa, H., Thompson, G. L., and Thrall, R. M., "The Double Description Method," in *Contributions to the Theory of Games*, vol. 2, H. W. Kuhn and A. W. Tucker, Eds. Princeton, NJ: Princeton University Press, 1953.
- [18] Bremner, D., Fukuda, K., and Marzetta, A., "Primal-Dual Methods for Vertex and Facet Enumeration," *Discrete Computational Geometry*, vol. 20, pp. 333-357, 1998.
- [19] Fukuda, K. and Prodon, A., "Double Description Method Revisited," in *Combinatorics and Computer Science*, vol. 1120, *Lecture Notes in Computer Science*, M. Deza, R. Euler, and I. Manoussakis, Eds. Springer-Verlag, pp. 91-111, 1996.
- [20] Nemhauser, G. L. and Wolsey, L. A., *Integer and Combinatorial Optimization*. New York: John Wiley, 1988.
- [21] Avis, D., "Computational Experience with the Reverse Search Vertex Enumeration Algorithm," *Optimization Methods and Software*, vol. 10, pp. 107-124, 1998.
- [22] Fukuda, K., "Note on New Complexity Classes ENP, EP and CEP - an Extension of the Classes $NP \cap Co-NP$ and P," ETH Zürich, Institute for Operations Research, Zürich June 12, 1996 1996.
- [23] Paul, B., *Kinematics and Dynamics of Planar Machinery*. Englewood Cliffs, NJ: Prentice-Hall Inc., 1979.